The Journal of Undergraduate Research in Physics

CONTENTS

VOLUME 4, NUMBER 2

WINTER 1985

Published by Guilford College
for
The American Institute of Physics and The Society of Physics Students

THE JOURNAL OF UNDERGRADUATE RESEARCH IN PHYSICS

This journal is devoted to research work done by undergraduate students in physics and its related fields. It is to be a vehicle for the exchange of ideas and information by undergraduate students. Information for students wishing to submit manuscripts for possible inclusion in the Journal follows.

ELIGIBILITY

The author must have performed all work reported in the paper as an undergraduate. The subject matter of the paper is open to any area of pure or applied physics or physics related field.

SPONSORSHIP

Each paper must be sponsored by a full-time faculty member of the department in which the research was done. A letter from the sponsor to the editor must accompany the manuscript if it is to be considered for publication.

FORM

The manuscript should be typed, double spaced, on 8 1/2 x 11 inch sheets. Margins of about 1 1/2 inch should be left on the top, sides, and bottom of each page. Papers should be limited to twelve pages of text in addition to an abstract and appropriate drawings, pictures, and tables.

GENERAL STYLE

All papers must conform to the Style Manual of the American Institute of Physics. Each paper must be prefaced by an abstract that does not exceed 250 words.

ILLUSTRATIONS

Line drawings should be made with black India ink on plain white paper. If a graph is drawn on co-ordinate paper, the paper must be lined blue. Important lines should be ruled in black. Each figure or table must be on a separate sheet. Photographs must have a high gloss finish.

CAPTIONS

A brief caption should be provided for each illustration or table, but it should not be part of the figure. They should be listed together at the end of the manuscript.

EQUATIONS

Equations should appear on separate lines and may be written in black India ink.

FOOTNOTES

Footnotes should be typed double spaced and grouped together in sequence at the end of the manuscript.

SUBMISSION

Two copies of the manuscript and a letter from the sponsor should be sent to:
Dr. Rexford E. Adelberger, Editor
THE JOURNAL OF UNDERGRADUATE RESEARCH IN PHYSICS
Physics Department
Guilford College
Greensboro, NC 27410

SUBSCRIPTION INFORMATION

The Journal will be published biannually with issues appearing in Summer and Winter of each year. There will be two issues per volume.

TYPE OF SUBSCRIBER	PRICE PER VOLUME
Individual	$ 5.00
Institution	$10.00

Foreign subscribers add $2.00 for surface postage, $10.00 for air postage.

To receive a subscription, send your name, address, and check made out to The Journal of Undergraduate Research in Physics (JURP) to:

Journal of Undergraduate Research in Physics
Physics Department
Guilford College
Greensboro, NC 27410

BACK ISSUES

Back issues may be purchased by sending $10.00 per volume to the editorial office.

ISSN 0731 - 3764

The Journal of Undergraduate Research in Physics is published by Guilford College for the American Insititute of Physics and the Society of Physics Students.

ELECTROMAGNETIC FIELD MOMENTUM DENSITY WITH MAGNETIC CHARGE PRESENT

Warren E. Levins *
Physics Department
Furman University
Greenville, SC 29613

ABSTRACT

One can derive from Maxwell's equations that the electromagnetic field produced by a charge configuration carries momentum. The same expression for the momentum density is obtained if part of the configuration is assumed to be a magnetic charge. This result is known, although both it and the standard proof, which are in covariant notation, are not generally accessible to undergraduate students. We prove that the form of the momentum density does not change when magnetic charge is introduced into the charge configuration using standard vector notation.

INTRODUCTION

The momentum density $\overline{p} \in \overline{R}^3$ (where $\overline{R}^3$ denotes a three-dimensional Euclidean real inner-product space) in the electric and magnetic fields produced by a charge configuration is:

$$\overline{p} = \mu_0 \epsilon_0 \overline{S} \tag{1}$$

where:

$$\overline{S} = 1/\mu_0 \ \overline{E} \times \overline{B} \tag{2}$$

is Poynting's Vector. Equation 1 is inferred from the classical expression for momentum conservation which is derived from the force equation for a charge moving in an electromagnetic field and from Maxwell's equations.

Two of Maxwell's equations:

$$\overline{\nabla} \cdot \overline{B} = 0 \qquad \overline{\nabla} \times \overline{E} = - \frac{\partial \overline{B}}{\partial t} \tag{3}$$

are incorrect if any part of the charge configuration is magnetic charge. The momentum density, however, is correctly given by Equation 1 even in that situation. This result is known, but the standard proof employs Maxwell's equations in covariant form. The following proof is in the more familiar vector notation.

THE PROOF

Suppose that in addition to an electric charge density ρ in a volume $V' \subseteq \overline{R}^3$, we also have a volume V'' holding a magnetic charge of density η. If $\overline{E}$ and $\overline{B}$ denote the net electric and magnetic fields, Maxwell's equation are usually generalized as (1):

$$\overline{\nabla} \cdot \overline{E} = \rho / \epsilon_0 \tag{4}$$

$$\overline{\nabla} \cdot \overline{B} = \mu_0 \eta \tag{5}$$

$$\overline{\nabla} \times \overline{E} = - \mu_0 \overline{K} - \frac{\partial \overline{B}}{\partial t} \tag{6}$$

$$\overline{\nabla} \times \overline{B} = \mu_0 \overline{J} + \mu_0 \epsilon_0 \frac{\partial \overline{E}}{\partial t} \tag{7}$$

where $\overline{J}$ and $\overline{K}$ are the electric and magnetic current densities. One can only postulate the force law for a magnetic charge moving with velocity $\overline{v}' \in \overline{R}^3$ to take on the form (2):

$$\overline{F_m} = \frac{d\overline{P}_m}{dt} = \int_{V''} (\overline{B} - \mu_0 \epsilon_0 \overline{v}' \times \overline{E}) \eta \ d\tau'' \tag{8}$$

in analogy to the electrical force law:

$$\overline{F_e} = \frac{d\overline{P_e}}{dt} = \int_{V'} (\overline{E} + \overline{v} \times \overline{B}) \rho \ d\tau' \tag{9}$$

If $V = V' \cup V''$ and the total mechanical momentum of the particles in volume V is:

$$\overline{P} = \overline{P_m} + \overline{P_e} \tag{10}$$

It follows then that:

$$\frac{d\overline{P}}{dt} = \frac{d\overline{P}_m}{dt} + \frac{d\overline{P}_e}{dt} \qquad (11)$$

The total force exerted on the system can be found by adding Equations 8 and 9 which yield:

$$\overline{F} = \frac{d\overline{P}}{dt} = \int_V (\rho\overline{E} + \eta\overline{B} + \overline{J}\times\overline{B} - \mu_0\epsilon_0\overline{K}\times\overline{E})\, d\tau \qquad (12)$$

Part of this expression for the force can be simplified by substituting in Equations 4 and 7 to give:

$$\rho\overline{E} + \overline{J}\times\overline{B} = \epsilon_0(\overline{\nabla}\cdot\overline{E})\overline{E} + 1/\mu_0[\overline{\nabla}\times\overline{B} - \epsilon_0\frac{\partial\overline{E}}{\partial t}]\times B \qquad (13)$$

The vector calculus identity:

$$\frac{\partial}{\partial t}[\overline{E}\times\overline{B}] = \frac{\partial\overline{E}}{\partial t}\times\overline{B} + \overline{E}\times\frac{\partial\overline{B}}{\partial t} \qquad (14)$$

can be transformed as:

$$\epsilon_0\frac{\partial\overline{E}}{\partial t}\times\overline{B} = \epsilon_0\left[\frac{\partial}{\partial t}(\overline{E}\times\overline{B}) - \overline{E}\times\frac{\partial\overline{B}}{\partial t}\right] \qquad (15)$$

Rewriting Faraday's law (Equation 6) gives:

$$\frac{\partial\overline{B}}{\partial t} = -[\overline{\nabla}\times\overline{E} + \mu_0\overline{K}] \qquad (16)$$

Substituting equations 15 and 16 into Equation 13 yields:

$$\rho\overline{E} + \overline{J}\times\overline{B} = \epsilon_0\left[(\overline{\nabla}\cdot\overline{E})\overline{E} - \overline{E}\times(\overline{\nabla}\times\overline{E})\right] - 1/\mu_0\overline{B}\times(\overline{\nabla}\times\overline{B}) - \mu_0\epsilon_0\overline{E}\times\overline{K} - \epsilon_0\frac{\partial}{\partial t}(\overline{E}\times\overline{B})$$

This equation can be further simplified by using the following identities. Multiplying both sides of Equation 5 by the magnetic field $\overline{B}$ gives:

$$1/\mu_0(\overline{\nabla}\cdot\overline{B})\overline{B} = \eta\overline{B} \qquad (18)$$

The vector calculus identity:

$$\nabla[D^2] = 2[\overline{D}\cdot\overline{\nabla}]\overline{D} + 2[\overline{D}\times(\overline{\nabla}\times\overline{D})] \qquad (19)$$

can be used to show that:

$$\overline{E}\times(\overline{\nabla}\times\overline{E}) = 1/2\,\overline{\nabla}(E^2) - (\overline{E}\cdot\overline{\nabla})\overline{E}$$
$$\overline{B}\times(\overline{\nabla}\times\overline{B}) = 1/2\,\overline{\nabla}(B^2) - (\overline{B}\cdot\overline{\nabla})\overline{B} \qquad (20)$$

Using equations 18 and 20 in Equation 17 gives:

$$\rho\overline{E} + \overline{J}\times\overline{B} + \eta\overline{B} - \mu_0\epsilon_0\overline{K}\times\overline{E} = \epsilon_0[(\overline{\nabla}\cdot\overline{E})\overline{E} + (\overline{E}\cdot\overline{\nabla})\overline{E}] + 1/\mu_0[(\overline{\nabla}\cdot\overline{B})\overline{B} + (\overline{B}\cdot\overline{\nabla})\overline{B}] - 1/2\,\overline{\nabla}[\epsilon_0E^2 + 1/\mu_0B^2] - \epsilon_0\mu_0\frac{\partial\overline{S}}{\partial t}$$

where $\overline{S}$ is the Poynting Vector.

We can simplify Equation 21 with Maxwell's stress tensor $\underset{\sim}{T}$. This tensor is defined as:

$$\underset{\sim}{T}_{ij} = \epsilon_0[E_iE_j - 1/2\,\delta_{ij}E^2] + 1/\mu_0[B_iB_j - 1/2\,\delta_{ij}B^2] \qquad i,j,k \in \{1,2,3\} \qquad (22)$$

The jth component of the divergence of the stress tensor ($j \in 1,2,3$) is:

$$\epsilon_0[(\overline{\nabla}\cdot\overline{E})E_j + (\overline{E}\cdot\overline{\nabla})E_j - 1/2\,\nabla_jE^2] + 1/\mu_0[(\overline{\nabla}\cdot\overline{B})B_j + (\overline{B}\cdot\overline{\nabla})B_j - 1/2\,\nabla_jB^2] \qquad (23)$$

(The "inner product" of a tensor and a regular vector can be defined through matrix multiplication. The nine elements of the tensor define a 3x3 matrix. The regular vector is a 3x1 column matrix. The "inner product" is just the matrix multiplication of these two matrices. In this way, one can work out the elements of the divergence of the Maxwell stress tensor.)

Equation 21 then can be rewritten using the divergence of the Maxwell stress tensor as:

$$\rho\overline{E} + \eta^- + \overline{J}\times\overline{B} - \epsilon_0\mu_0\overline{K}\times\overline{E} = \overline{\nabla}\cdot\underset{\sim}{T} - \epsilon_0\mu_0\frac{\partial\overline{S}}{\partial t} \qquad (24)$$

Recalling that the net force is just the integral of Equation 24 over all space, one may write:

$$\frac{d\overline{P}}{dt} = \int_V(\overline{\nabla}\cdot\underset{\sim}{T} - \epsilon_0\mu_0\frac{\partial\overline{S}}{\partial t})\, d\tau \qquad (25)$$

Using the Gauss divergence theorem, Equation 25 becomes:

$$\frac{d\overline{P}}{dt} = -\epsilon_0\mu_0\frac{\partial}{\partial t}\int_V \overline{S}\, d\tau + \int_{\partial V} \underset{\sim}{T}\cdot d\underset{\sim}{a} \quad (26)$$

Where ∂V denotes the boundary of V. One identifies the first term of this equation as the rate at which the field momentum inside the volume V is changing and the second as the rate of change through the boundary. This suggests that the momentum density of the fields can be written as:

$$\overline{p} = \epsilon_0\mu_0\,\overline{S} \quad (27)$$

REFERENCES

* Present address: Department of Physics, University of California, Davis, CA 95616

(1) Rohrlich, F., Phys. Rev. 150, 1104, 1966.

(2) Griffiths, D.J., Introduction to Electrodynamics, Prentice-Hall, Englewood Cliffs, NJ, 1981, p.277

FACULTY SPONSOR OF THIS PAPER

Dr. Frank C. Taylor
Physics Department
Furman University
Greenville, SC 29613

A NUMERICAL APPROXIMATION TO THE QUANTUM MECHANICAL SOLUTION FOR THE ENERGY EIGENFUNCTIONS OF THE SODIUM ATOM

Michael Lawson
Physics Department
Guilford College
Greensboro, NC 27410

ABSTRACT

The time-independent Schrodinger wave equation for single-valence electron atoms was reduced to a dimensionless form in order to facilitate computer manipulation. An approximation to the radial charge density of the core of the sodium atom was used to modify the potential energy term of the dimensionless equation. Energy eigenvalues and bound wavefunction solutions were found using a fifth-order Runge-Kutta program. The energy levels found agreed closely with the accepted values for the sodium atom.

INTRODUCTION

The time-independent Schrodinger equation for a spherically symmetric potential can be written as:

$$-\frac{\hbar^2}{2m}\nabla^2\psi + V(r)\psi = E\psi \qquad (1)$$

The radial part of equation 1 is all that is needed to determine the energy eigenvalues. Substituting in the radial part of the Laplacian operator and using separation of variables yields:

$$-\frac{\hbar^2}{2mr^2}\frac{d}{dr}\left[r^2\frac{dR}{dr}\right] + \left[V(r) - \frac{l(l+1)\hbar^2}{2mr^2}\right]R = ER \qquad (2)$$

where R is the radial component of the wavefunction, l is the angular momentum quantum number, and V(r) is the potential representing the attractive interaction between the electron and the nucleus. The equation for the angular components of the wavefunction can be found elsewhere (1). Equation 2 can be simplified further by making the following substitution:

$$R(r) = U(r)/r \qquad (3)$$

Equation (2) then becomes:

$$-\frac{\hbar^2}{2m}\frac{d^2U}{dr^2} + \left[\frac{l(l+1)}{2mr^2} - V(r)\right]U = EU \qquad (4)$$

To be able to use this equation in a computer program, one must reduce it to a dimensionless form to avoid overflow errors due to the extremely large and extremely small numbers in the equation. This can be done using the following substitutions:

$$r = a_0\rho \quad a_0 = \hbar^2/me^2$$

$$E = E_r\epsilon \quad E_r = me^4/2\hbar^2 \qquad (5)$$

$$V = WE_r$$

which yields:

$$\frac{d^2U}{d\rho^2} = \frac{l[l+1]}{\rho^2}U - \frac{2W}{\rho}U - \epsilon U \qquad (6)$$

a dimensionless equation where ρ and ϵ are unitless values and approximately equal to 1, making computer solutions feasible.

MODELING THE POTENTIAL

The task at hand was to model a function that would give us an approximation to the true potential experienced by the outer electron of the sodium atom. It surely must be different from a simple coulomb function as the energy spectrum of sodium is significantly different from that of hydrogen. The potential can be approximated as:

$$W = Z - \sigma[\rho] \qquad (7)$$

where Z is the number of protons and is the screening constant that is dependent on the charge density of the inner electrons of the K and L shells. The K shell contains 2 electrons and the L shell 8.

The measured radial charge density for the sodium atom is shown in Figure 1. One must make a model of this with analytic functions if Runge-Kutta is to be used to solve Equation 6. This was accomplished by dividing the graph into two parts, one for the K shell and one for the L shell. The K shell density was approximated by:

$$\sigma_k \cong 1 - \cos[2\pi\rho] \quad 0 \leqslant \rho \leqslant .5 \qquad (8)$$

while the L shell was approximated by:

$$\sigma_l \cong 1.27\pi\{1-\cos[.838\rho]\} \quad \rho \leqslant 3.75 \qquad (9)$$

The integral of each function over the limits given must equal the number of electrons in that shell. The dotted line in Figure 1 is a plot of the sum of these two functions and compares them with the true density.

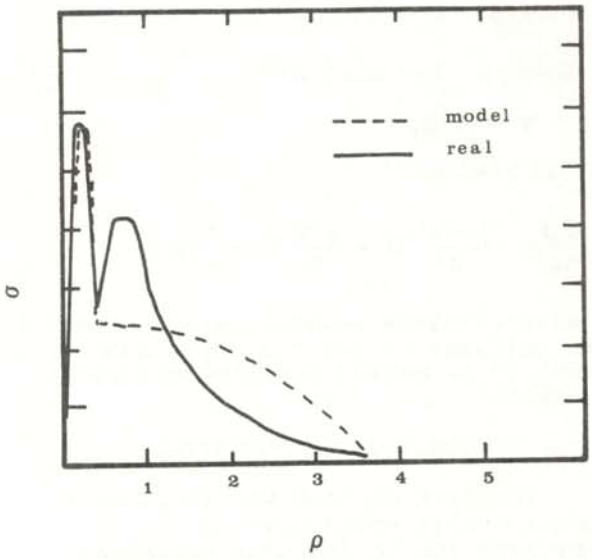

FIGURE 1
The charge density as a function of ρ for sodium. The solid line is fom H.E. White, Introduction to Atomic Spectra, McGraw-Hill, 1934, p. 103. The dotted line is the functions used to model the potential.

Placing this approximation to the radial charge density into Equation 7 gives:

$$\frac{d^2U}{d\rho^2} = \frac{l[l+1]}{\rho^2} U - \frac{2}{\rho}\{\sigma_l+\sigma_k\} - \epsilon U \qquad (10)$$

This unitless form of Schrodinger's equation approximates the behavior of the valence electron of the sodium atom. It is also in a form that can be readily solved using the Runge-Kutta algorithm for a given l state and energy eigenvalue.

THE PROGRAM

The numerical calculations were done using a fifth-order Runge-Kutta algorithm and written in BASIC for a DEC VAX750. A derivation for this method can be found elsewhere (2). The algorithm calculated a value for U(k+1) from U(k). To start the procedure, one must input the initial U, $dU/d\rho$, and initial and final values of ρ . One must also input the desired angular momentum quantum number and energy eigenvalue. A listing of the program can be obtained from the Guilford College Physics Department.

Using this algorithm, a solution for any energy and angular momentum can be found. However, only those that are bounded exist in the physical world. The bounded solutions were found by using the Runge-Kutta routine to find the value of the wavefunction for large values of ρ . In most cases, these solutions diverged as ρ increased. The energy eigenvalue was then increased and the routine run again. If U changed from diverging negatively to diverging positively or vice-versa, a bounded state (where U approaches 0 as ρ gets large) must be between these two values. Once a bounded state was bracketed, the interval in the energy search was cut in half until the desired uncertainty in the energy eigenvalue was achieved.

An example to explain this procedure is given below. For a given l-state, the first input for energy might be 0. The solution to Equation 10 might oscillate to a particular value of ρ and then diverge positively at an exponential rate. The next input for energy (keeping the value of L fixed) would then be 1. If the value of U oscillates and then diverges negatively, we know that there was an energy eigenstate between 0 and 1. The next

input for energy would then be .5. If this causes U to diverge positively, it is concluded that the energy eigenvalue is between .5 and 1. If this procedure is repeated a sufficient number of times, any desired precision can be achieved.

The output from the Runge-Kutta program was used in a graphics program to display graphs of U versus ρ for the different energy states found. The values of the principle quantum number were assigned to the various states by counting the number of peaks in the solution for U and adding it to 1.

RESULTS AND CONCLUSIONS

Table 1 gives a list of the energy states found, their accepted values, and the computed values obtained from the simulation with a precision of .01 eV. Figure 2 shows plots for the energy states 3p, 4f, 5s and 5d. On each graph are plotted two sets of data; one for the energy value that causes a positive divergence, and the other for the energy level that causes negative divergence. The 5s graph has a peak near $\rho = 0$ which does not show up well.

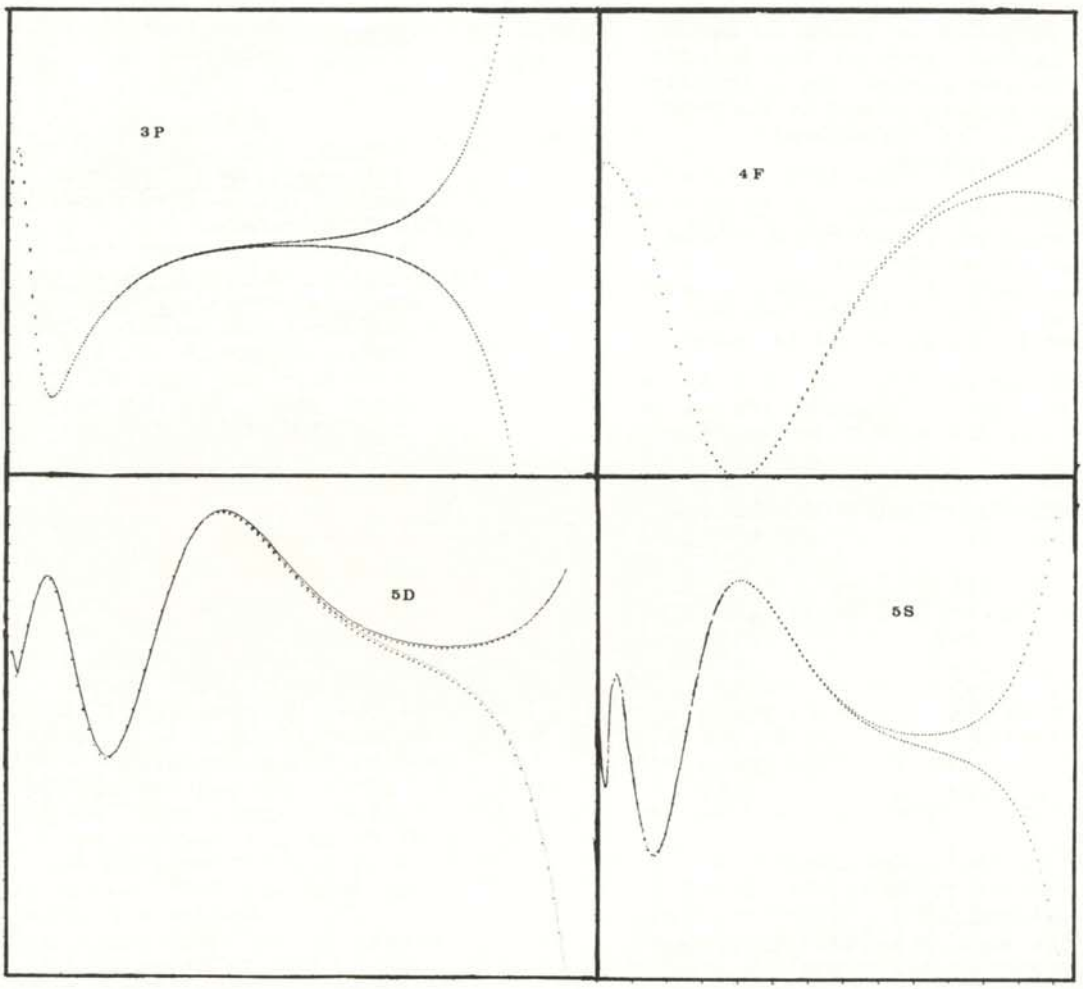

FIGURE 2
Results of the calculations. Each set is for an energy where the wavefunction diverges positively and for the next energy chosen where the wavefunction diverges negatively. There is a small peak on the 5s graph near $\rho = 0$ that does not show up well.

This simulation shows that the model of the radial charge-density of the inert core electrons and the procedure for finding the bounded wavefunctions can be used to find the energy levels of sodium. The energy states were, on the average, within 2 percent of the accepted values. The computed energy values for those states for which the valence electron was outside the inert core electron (d or f states) were closer to the accepted values than those where the valence electron interacted with the inert core electrons. This can be attributed, in part, to the inaccuracy of the model of the charge density. For the 5d and 4f states, an extra peak was found near the origin. This is believed to be an artifact of faulty input of the initial conditions for the slope. An initially negative slope should give the correct number of peaks. This hypothesis, however, was not tested.

A possible improvement of this simulation would be to design a better model for the charge-density distribution, possibly including a term for the spins, such that the results for the lower l states would be more accurate.

STATE	EXPERIMENTAL eV	THEORETICAL eV
3S	5.15	5.13
4S	1.89	1.93
5S	.997	1.01
6S	.615	.614
3D	1.43	1.51
3P	2.96	3.02
4D	.809	.837
4F	.848	.835
5D	.530	.521

TABLE 1
List of the energy states found in the numerical search. The accepted values for these states are also listed.

ACKNOWLEDGMENTS

The author would like to thank Thom Espinola, Sheridan Simon, and Rexford Adelberger, all of Guilford College, for their help with this simulation.

FACULTY SPONSOR OF THIS PAPER
Thom Espinola
Physics Department
Guilford College
Greensboro, NC 27410

REFERENCES

(1) French, A.P., and E.F. Taylor, An Introduction to Quantum Physics, Norton & Co., Inc., New York, 1978, p. 201.

(2) McCann, R.C., Introduction to Ordinary Differential Equations, Harcourt, Brace, Janovich, Inc., 1982, p. 308.

MEASURING THE LIFETIME OF A METASTABLE STATE IN AN OPTICAL MATERIAL*

Donald J. Schertler
Physics Department
Thomas More College
Crestview Hills, KY 41017

ABSTRACT

The lifetime of a metastable state of a ruby crystal was measured by observing the decay rate of the intensity of the emitted light from the excited optical material. The light intensity was converted to an electrical signal, digitized with an Analog to Digital converter and then analyzed with an Apple II+ computer.

INTRODUCTION

The applicability of an optical material for use as a medium for a laser is dependent upon the existence of a metastable or long lived (0.1 - 10 msec) state in the material. Several common laser materials have easily measurable spontaneous emission lifetimes. Such materials include ruby and neodynium (Nd) in both the YAG and glass hosts. The relative ease of the measurement of this lifetime (1) as well as the simplicity of the fundamental theory regarding the emission makes it ideal for use as a sophomore level laboratory exercise.

THEORY

Energy is optically pumped into the reacting atoms. These atoms are raised into excited states by what are called the pump or absorption bands. Then a fast non-radiative decay process (such as a collision) populates the upper metastable laser level. This metastable state becomes polulated in a very short time compared to the decay time of this state. The electron in this metastable state then spontaneously drops down to the ground state with the emission of the characteristic laser radiation photon. It is the lifetime of the emission that is measured in this experiment.

Ruby crystals and Nd glass absorb light in the visible range and emit it in the .65 to 1.06 micron range (2). The excited atoms which absorb the visible photons and ultimately populate the metastable level decay exponentially with time to a lower energy level. The population of the excited state is:

$$N[t] = N_0 \exp[-t/\lambda] \qquad (1)$$

where N(t) is the population at time t, N_0 is the initial population and λ is the lifetime of the excited state. Since each decay from the metastable level gives off a photon, the intensity, I(t), of the emitted light is given by:

$$I[t] = -\frac{dN}{dt} = \frac{N_0}{\lambda} \exp[-t/\lambda] = \frac{N[t]}{\lambda} \qquad (2)$$

A plot of the natural logarithm of the light intensity versus time can be used to determine the lifetime λ of the metastable state.

APPARATUS AND EXPERIMENTAL PROCEDURE

A strobe light, set at about 10 - 15 Hz, is the pumping source for the lasing material. The sample is clamped in a small box which is light tight except for a small tapered hole which allows the light from the strobe to enter and excite the sample (see Figure 1). A phototransistor (3) is used to detect the light emitted from the sample.

A function generator (4), external to the computer, determines the time interval between data points taken by the Analog to Digital (A/D) converter

card (5) within the Apple II+ computer. The generator sends a pulse to a buffer circuit (see Figure 2) which initiates a machine language program to take a data point. A BASIC language program then graphs the points on the monitor so that the decay can be isolated and stored in a text file for further analysis (6).

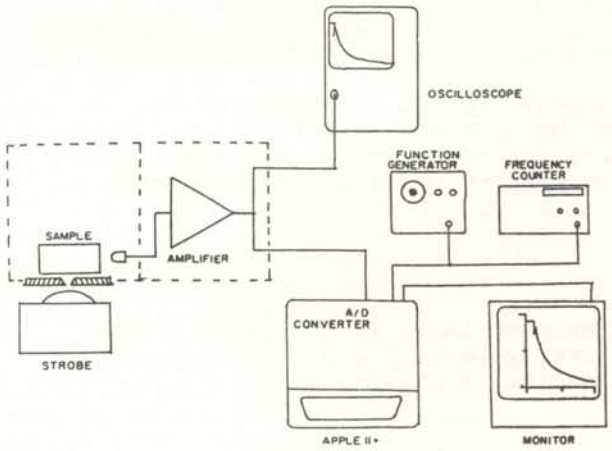

FIGURE 1
Equipment configuration. The dashed line represents the light-tight box containing the crystal and amplifier circuit.

The A/D converter digitizes voltages in the range +5 volts to - 5 volts to the values 255 and 000 respectively. The greatest precision is obtained by using this entire voltage range. Thus an amplifier which would place the analog voltage from the phototransistor that measures the light intensity within this range is needed.

Such a circuit (3) put the peak voltage (maximum intensity) of the decay at about 0.8 volts. This range precluded measurements using the computer. The output of the amplifier could be increased by increasing the intensity of the pumping light, but other difficulties are caused by this increase. Figure 3, showing the oscilloscope trace for a high intensity, shows this well. The clipped portion indicates that the strobe intensity exceeds the range of the amplifier. The major concern, however, is the ringing which occurs after the clipped portion. This indicates that the circuit is unstable.

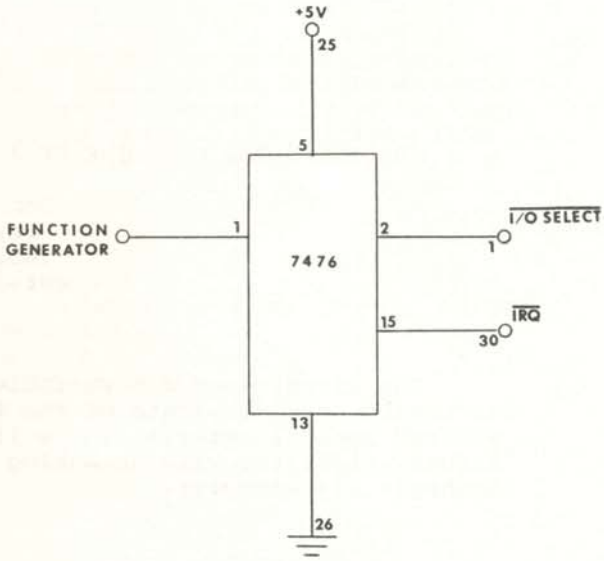

FIGURE 2
Buffer circuit which interfaces the function generator to the computer. The diagram shows the chip connections and the connections to the I/O port of the Apple II+.

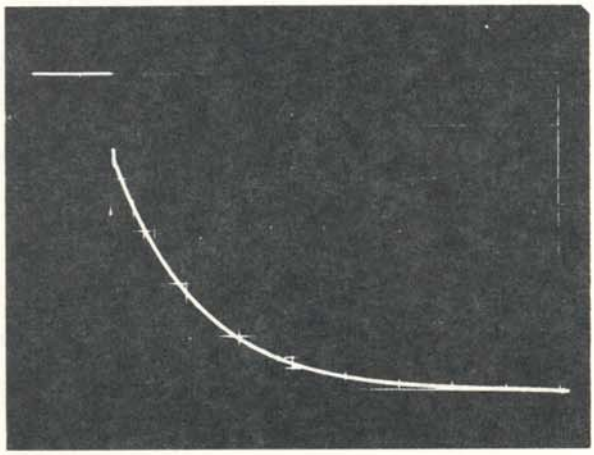

FIGURE 3
Oscilloscope trace of the output from Feinberg's circuit using a ruby crystal. Scale readings are: 1 Volt/division vertical, and 2.0 msec/division horizontal. The entire decay is shifted about 1 volt above the zero volt mark.

Furthermore, the entire decay is shifted by about 1 volt DC above the zero volt mark, putting it out of the

range of the A/D converter. This would be acceptable if only an oscilloscope measurement is desired. Using the oscilloscope technique gives a value of $3.2 \pm .1$ msec for the life time of the metastable state in the ruby crystal. However, the problems associated with this circuit make data logging on the computer impossible. For a more precise measurement of the decay rate, a more stable and adjustable circuit design is needed.

A new circuit design which allows for maximum control over the output is shown in Figure 4. The adjustable voltage biasing (R1) to the phototransistor gives control over the signal sent to the operational amplifier (6). The DPDT switch enables one to select two outputs: 1) the phototransistor, to adjust its voltage; or 2) the circuit output to take data. The gain (R3) and DC offset (R2) give control over the voltage range of the circuit output. This allows the entire range, +5 to -5 Volts, of the A/D converter to be used. Figure 5, a photograph of the oscilloscope trace of the output of the new amplifier, shows that there is no ringing and that the output spans the +5 to -5 Volt range (the 0 Volt make corresponds to the center line). The output of the amplifier circuit is sent to the A/D converter and digitized.

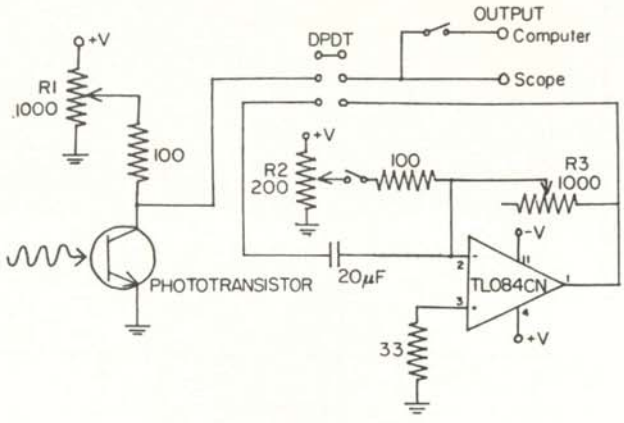

FIGURE 4
Modified amplifier circuit diagram showing the adjustable voltage biasing of the phototransistor (R1), the DC offset (R2), and gain (R3) controls. All resistances are in KOhms.

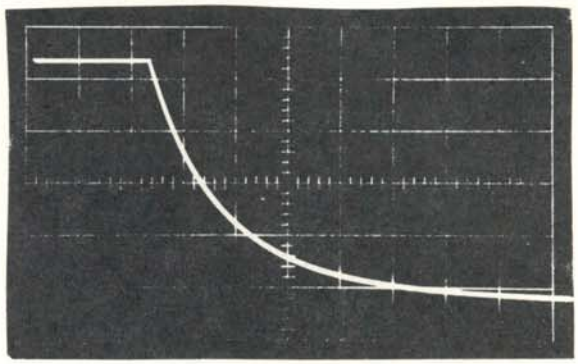

FIGURE 5
Oscilloscope trace of the output of the modified amplifier circuit for the decay of the metastable state of a ruby crystal. The scale readings are: 2volts/division vertical and 2.0 msec/division horizontal, with the 0 volt mark in the center.

Initially an input resistor was included in the circuit shown in Figure 4. Since most amplifiers of this type have a resistor input, one was included between the capacitor and the feedback junction. This had the effect of adding an RC decay to the light intensity decay of the crystal. Only after much investigation and manipulation of the original amplifier circuit was the cause of the additional decay discovered.

ANALYSIS AND RESULTS

The computer generated graph of the decay of the metastable state in ruby, shown in Figure 6, is a copy of the graph seen on the monitor. It is generated by a BASIC program. The Y-axis corresponds to the digitized value of the intensity. It is important to note that the zero reference level of the decay may not correspond to the zero mark on the Y-axis due to the adjustable DC offset of the amplifier. The zero adjustment of the decay data is done with another BASIC program.

The X-axis of Figure 6 corresponds to the time interval from the exciting flash to when the data is taken. The conversion of this scale to time is done using the frequency of the function generator. A frequency of 10.000 KHz gives 0.1000 msec between successive data points. Thus the X-axis range, 770

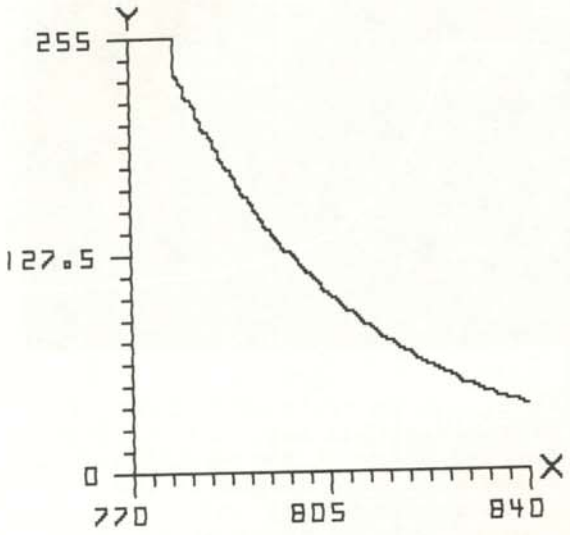

FIGURE 6
Computer generated graph of the decay of the metastable state of the ruby crystal. The time between points is .100 msec giving a time span of 7.00 msec.

to 840 is a time span of 7.000 msec. This graphing technique is used only to isolate the decay from the other points, store them in a data file, and to determine the zero reference point of the decay.

Equation 2 can be rewritten as:

$$\ln\left\{I[t]\right\} = \frac{-t}{\lambda} + \text{¢} \qquad (3)$$

Figure 7 is a plot of the natural logarithm of the intensity versus time for a ruby crystal. The straight line indicates that the simple theory applies. A BASIC program with a least squares fit routine used to determine the slope of this line yielded a value of 3.200±.005 msec for the lifetime of the metastable state. This is a sharp increase in the precision of the measurement found from the oscilloscope trace.

Fifteen measurements of the decay rate were taken to determine the reproducibility of the results when the gain and adjustable voltage biasing of the amplifier were varied. The values ranged from 3.168 msec to 3.213 msec with an average value of (3.19±.02) msec.

CONCLUSIONS

The use of an A/D converter and the Apple II+ Computer has enabled us to obtain a high degree of precision in the measurement of the lifetime of the metastable state of a ruby crystal. The lifetime found in the literature (2,8) is 3 msec. With this method, a value of (3.19±.02) msec was obtained.

The development of the amplifier circuit consumed much of the time spent on the project. It is one of the more significant accomplishments of this project. The application of this circuit design (Figure 5) is not limited to just this experiment, but is suitable for analysis of any time dependent signal by a computer and any A/D converter having a limited voltage range.

ACKNOWLEDGMENTS

The author is indebted to Kevin Cahill, a student at Thomas More College, for his design of the buffer circuit and accompanying machine language program. He is wishes to acknowledge Jack Wells of Thomas More College and Dexter Clark of the University of Cincinnati for their advice and suggestions. The author would also like to thank J.H. Meyer of Hughes Aircraft Company for the donation of the ruby crystal.

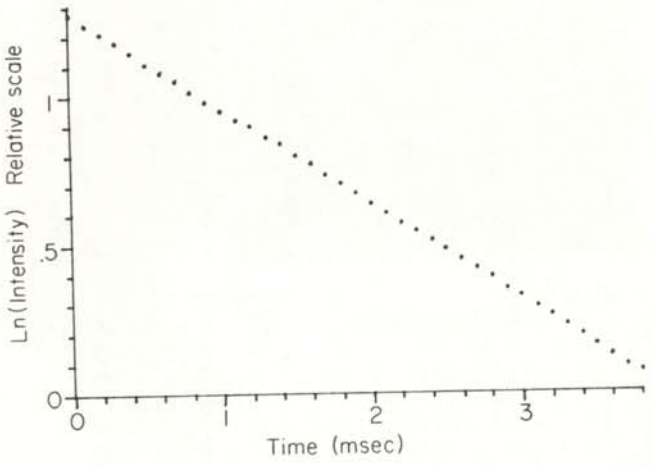

FIGURE 7
Plot of the natural logarithm of intensity versus time for the decay of the metastable state of a ruby crystal. The least squares fit slope of 1312.4 sec gives a lifetime, λ, of 3.200 msec.

REFERENCES

* This research was supported by the Society of Physics Students through an Allied Award.

(1) Feinberg, R., "Measuring the Lifetime of a Metastable State", Am. J. of Phys., 51, 573, 1983

(2) For pertinent energy level diagrams see: Hecht, J., "The Neodynium Laser", Lasers and Applications, 2, 57, Nov. 1983; Yariv, A., Introduction to Optical Electronics, 2nd Ed., Holt, Rinehart, and Winston, New York, 1976.

(3) Phototransistor available from Radio Shack (part # 276-130). Others will work just as well.

(4) Hewlett Packard Function Generator, Model 3310A. Any good function generator with a TTL output will work.

(5) Mountain Hardware A/D and D/A converter cards for the Apple II Computer. Mountain Computer Inc., 300 El Pueblo Road, Scotts Valley, CA 95066 (408)-438-6650.

(6) TL084CN OP AMP with a JFET input, available from any electronics supplier.

(7) The programs used in this project are available from the Physics Department, Thomas More College, Crestview Hills, KY 41017.

(8) Duchert, J., and R. Alfano, "Emerald - A New Gem Laser Material", Laser Focus, 19, 117, Sept. 1983.

FACULTY SPONSOR OF THIS PAPER

Jack Wells
Physics Department
Thomas More College
Crestview Hills, KY 41017

A MICROCOMPUTER CONTROLLED LASER SECURITY SYSTEM

John C. Cummings
Physics Department
Virginia Military Institute
Lexington, VA 24450

ABSTRACT

A microcomputer interface has been designed and constructed that will serve as an early warning system for intrusion of the perimeter of a command post. Interruption of laser beams, which define the perimeter at two different ranges, will result in computer generated signals that produce voice synthesized commands as well as a warning on a video terminal. A software handled interrupt has been used to deal with the situation where both beams are broken at or near the same time.

INTRODUCTION

A microcomputer interface has been constructed that will serve as an early warning system for the intrusion of the perimeter of a command post. Light is emitted from two lasers at the command post. These two light beams are directed outward to mirrors which reflect them around the command post perimeter at each of two different ranges (see Figure 1). Upon completion of a trip around the periphery, each beam is directed back to the command post and focused on separate phototransistors. Should either beam be broken, the corresponding phototransistor will generate a signal which can be detected by the microcomputer.

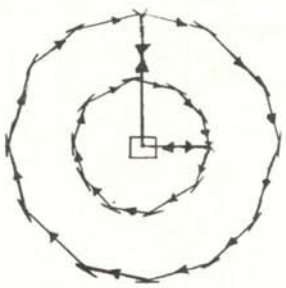

FIGURE 1
Schematic diagram of the path of the laser beams surrounding the command post (at the center of the diagram),

Upon detection of an intrusion, the program (1), written in BASIC, calls a subroutine to handle the generation of a message that is visually displayed and audibly given by a speech synthesis hardware device. While responding to a particular intrusion, the computer continues its surveillance to detect any breakage of the other light beam. Should a second intrusion occur while the first is being processed, an interrupt is produced which is subsequently handled by software. The second intrusion will not be processed before the command post operator has an opportunity to receive an audio signal whose frequency indicates which beam has been broken.

DETAILS OF THE SYSTEM

Photodetection System

The light beams are produced by 2 mW HeNe lasers (λ =632.8 nm). Upon returning to the command post, each beam is focused onto the light sensitive surface of a phototransistor by a converging lens. The phototransistor (2), shown in Figure 2, is sensitive to light of wavelengths in the visible range. When the light beam falls on the phototransistor, the output will be high (logic 1). When light no longer hits the sensitive surface, the phototransistor ceases to conduct enough current to keep the output from going low (logic zero). The output of each of the two phototransistors constitutes one of the two bits of information that the computer must read.

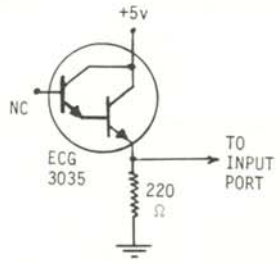

FIGURE 2
Schematic diagram of the phototransistor used to detect a break in the laser beam.

The computer

The system is controlled by a TRS-80 Model I computer with an interface unit (3) attached to connect it to the outside world. The data bus (8 lines), eight decoded address-select lines, the four least significant bits on the address bus and the necessary I/O signals are available on the interface unit.

Input/Output Port

The status of the two phototransistor detection circuits is determined by monitoring the logic states of each of the two output lines. This status information must be read by the computer, so there must be a tri-state input port. Information must be sent from the computer to the speech synthesis hardware, therefore an output port must also be available.

Both the input and output ports can be obtained by using an Intel 8255 programmable peripheral interface chip (PPI), an LSI device which can provide three 8-bit ports that can be programmed to select as either input or output. The 8255 PPI is wired as shown in Figure 3. The least significant address bits A0 and A1 select which port (A,B,C or Control Word) is active. The chip is selected when the $\overline{CS}$ line goes low. The $\overline{IN}$ and $\overline{OUT}$ lines (from the interface unit) coordinate the I/O operations of the chip.

The chip select ($\overline{CS}$) signal is generated when any of the addresses $\overline{4}$,$\overline{5}$,$\overline{6}$ or $\overline{7}$ are specified by the computer program. The decoded address signals (active low) are available on the interface unit. If data is to be input to the computer from the 8255 chip, it is necessary to generate an input request signal (a negative pulse) to reverse the direction of the bidirectional data bus buffer chips on the interface unit.

Speech Synthesis Hardware

Upon detection of a logic zero in either of the two least significant bits of Port A, the computer will print a message on the CRT display and proceed to activate the speech synthesis hardware, causing this circuitry to issue a pre-arranged message. The hardware is patterned after the DIGITALKER system (4). A Standard Vocabulary Kit and two speech ROMs were used to provide a total of 268 separate words, two different frequency tones and 5 different silence durations. The schematic diagram of this system, as obtained from the manufacturers literature, is shown in Figure 4.

The speech processor chip (see Figure 5) is controlled by a 3.579 Mhz crystal and the speech output line from the chip is used to drive an appropriate filter and amplifier circuit, which in turn drives the speaker.

THE PROGRAM

Interruption of either of the two light beams results in a logic zero at the corresponding bit of Port A. The program samples this port, and hence the status of the beams, every milisecond.

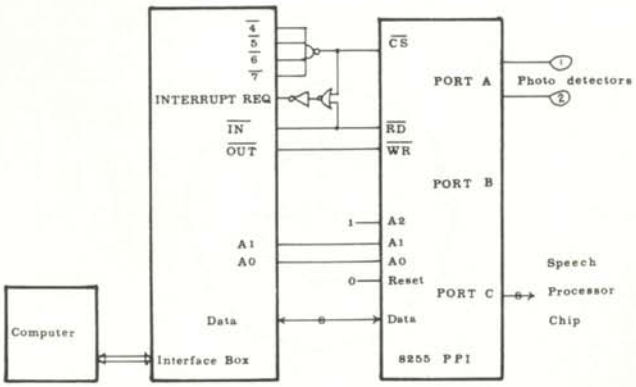

FIGURE 3
Schematic diagram of the logic used to control the 8255 PPI chip.

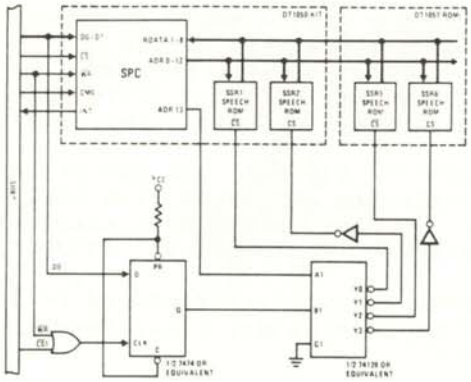

FIGURE 4
Schematic diagram of the DIGITALKER Speech Synthesis Circuit.

When a zero is detected, the computer is directed to the appropriate subroutine. Each subroutine causes the appropriate message to be displayed on the CRT and then successively selects which of the speech ROMs is to provide the next word, tone or pause. The selection of the specific ROM is detailed in Figure 6.

An OUT 1,0 command by the computer results in a negative pulse at the Clear (CLR) input of the flip-flop, thereby making the B1 input to the decoder low. This will result in either Y1 or Y0 being low, depending upon the A1 decoder input from the speech processor chip. If Y1 is low, then the 1050 ROMs are selected. On the other hand, the execution of an OUT 2,0 instruction will set the output of the flip-flop high and will thereby select the DT1057 ROM pair.

Once the correct pair of ROMs has been selected, the speech processor chip (SPC) is instructed by the computer to accept the address of the word to be used. The desired word is then obtained from the appropriate ROM (as determined by the A13 output from the SPC) and the SPC provides an analog output that represents the speech data. The analog signal is then filtered and amplified and ultimately drives the speaker. The "voice" output is an easily intelligible male voice.

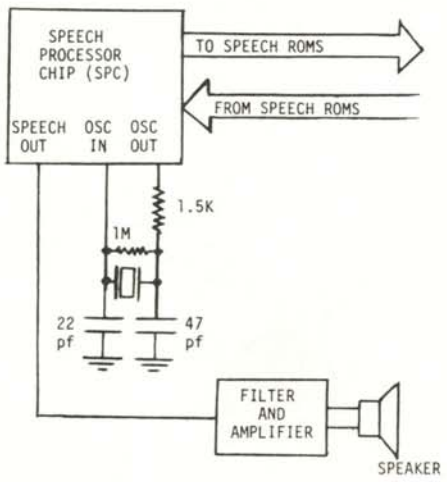

FIGURE 5
Schematic of the Speech Synthesis Circuit.

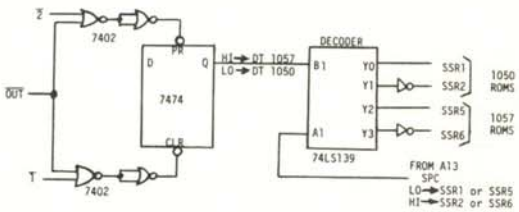

FIGURE 6
Circuit for selecting the correct ROM for use with the Speech Processor Chip.

The software controls the interval between the spoken words. The speech processing circuitry is given about .5 sec to complete each word, independent of the length of the word being spoken. This interval seems to be adequate, but the speech quality could probably be improved by using the interrupt line (INTR) on the SPC. This line goes high at the completion of any speech sequence. It is reset by the next valid command. Using this line to determine the time interval between words, a more fluid speech pattern could be achieved.

The software also provides an interrupt should the other beam be broken while the speech synthesis circuitry is producing a message. The check for a second break takes place as part of the software generated pause between successive words in the

message. An improvement in the procedure would involve delaying the second message until the first message had been completed.

A rarely occurring, but never-the-less not negligible "Glitch" was the sensing of a false break as a result of power line noise. One either has to be very careful to get a 5 volt power supply with a very high level of filtering or write a software debounce routine of the breaking of the beams. If a break in the beam is detected, wait a millisecond and then read it again to see if it is still broken. If so, record it, if not, ignore it. In this manner, one can get rid of the problem of fast spikes due to the power supply causing false beam break signals.

REFERENCES

(1) Listings of the BASIC programs that operate this system are available from the Physics Department, Virginia Military Institute, Lexington, VA, 24450.

(2) ECG3035 (2N5780), an NPN Photo Darlington available from AVEC Electronics Corp., 2002 Staples Mill Rd., Richmond, VA 23230.

(3) Model BG-101, manufactured by Group Technology, LTD., Cheek, VA. 24072.

(4) Model DT 1050 Standard Vocabulary Kit and two DT1057 speech ROMs, manufactured by National Semiconductor Company.

FACULTY SPONSOR OF THIS PAPER

Dr. Philip B. Peters
Department of Physics
Virginia Military Institute
Lexington, VA 24450